Research Journal of Applied Sciences, Engineering and Technology 7(10): 1985-1993, 2014
DOI:10.19026/ajfst.7.490
ISSN: 2040-7459; e-ISSN: 2040-7467

Submitted: June 17, 2013 Accepted: June 25, 2013 Published: March 15, 2014

Research Article

J-Integral Evaluation of Surface Cracks in Round Bar under Mode III Loadings

[1]A.E. Ismail, [2]A.K. Ariffin, [2]S. Abdullah and [2]M.J. Ghazali
[1]Faculty of Mechanical and Manufacturing Engineering, Universiti Tun Hussein Onn Malaysia, Baru Pahat, 86400 Johor, Malaysia
[2]Faculty of Engineering and Built Environment, Universiti Kebangsaan Malaysia, Bangi, 43500 Selangor, Malaysia

Abstract: Fracture mechanics approach has successfully used to characterize the existing cracks in engineering materials and structures. Tremendous number of publications on surface cracks can be found for crack behaviour which was assumed to behave linear elastic. However, lack of information on elastic-plastic crack behaviour or *J*-integral was demanded especially for 3D surface cracks. In this present study, semi-elliptical surface cracks embedded in a solid round bar subjected to mode III loadings are considered. Then, *J*-integral or *h*-function and limit load were determined and analyzed. In order to predict *J*-integral along the crack front, a mathematical model was then developed. It is found that the developed model capable to predict *J*-integral well. However, the predictions breakdown occurred when the elastic dominated region of cracks.

Keywords: ANSYS, J-integral, mode III loadings, round bar, surface crack

INTRODUCTION

Solid cylindrical bars are generally used as a shaft in engineering fields to transmit power from one point to another. Due to several factors such as material or design defects, the shaft can be experienced a mechanical failure over certain period of time. Such failure can be divided into three stages:

- Micro crack initiation
- Crack growth
- Final failure (Anderson, 2005)

Fracture mechanics is frequently used to characterize such failure. For linear-elastic materials, it is sufficient to use Stress Intensity Factor (SIF) to analyze the crack behaviour. If the plastic deformation is large, *J*-integral is used. Since the introduction of powerful computer between 1965 until 1979, various numerical methods are developed such as finite element method used to find the solution for SIFs. After 30 years of research, Toribio *et al.* (2009) summarized that the solution for SIFs have already covered all aspects of crack geometries which is not only concerned at the deepest crack point as well documented by Murakami and Tsuru (1987).

In fracture mechanics, SIF and J-integral is important in order to evaluate the reliability of crack structures. Recently, mode I SIFs has given more priority since its effect is significant compared with other types of SIFs for example mode II and III (Raju and Newman, 1982). Most researchers have concentrated their work on mode I SIFs since the introduction of numerical methods and it is well understood (Toribio *et al.*, 2009). However, there are lacks of solution for the SIFs obtained using mode II and III loadings significantly (Ismail *et al.*, 2012a). These two types of SIFs are important due to the fact that, the mode II and III SIFs also played an important role in determining the structural integrity.

According to literature survey (Fonte and Freitas, 1997; Shahani and Habibi, 2007; Ismail *et al*., 2012b), mode III SIFs has already been published previously. *J*-integral solution for mode I can be found in (Toribio *et al.*, 2009) for surface crack in a plate. However, lack of solution for *J*-integral for surface crack in round bars subjected to mode III loadings. Therefore, this study focused to determine and analyze the *J*-integral subjected to elastic-plastic mode III loadings.

J-integral estimation: *J*-integral firstly introduced by Rice (1968). Assuming a single edge crack embedded in a 2D elastic or elastic-plastic plate. *J*-integral is defined as an arbitrary curve around the crack tip and it is evaluated counter-clock wise as in Fig. 1 which can be expressed as:

$$J = \int_{\Gamma} \left(W dy - \vec{T} . \frac{\partial u}{\partial z} ds \right) \quad (1)$$

Corresponding Author: A.E. Ismail, Faculty of Mechanical and Manufacturing Engineering, Universiti Tun Hussein Onn Malaysia, Baru Pahat, 86400 Johor, Malaysia

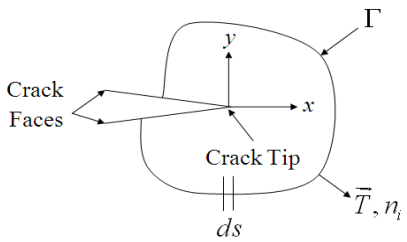

Fig. 1: Definition of the J-integral evaluation

where,
$\vec{T}$ = A traction vector defined as outward along the Γ
T_i = $\sigma_{ij}n_i$ or force per unit length
u = A displacement vector
ds = An element on curve Γ
W = A strain energy density expressed by:

$$W = \int_0^{\varepsilon} \sigma_{ij} d\varepsilon_{ij} = \int_0^{\varepsilon} \{\sigma\}^T d\{\varepsilon\} \quad (2)$$

where, ε_{ij} is strain tensor and $\{\varepsilon\}$ represents a strain vector. The path independent on J-integral has already proved by Rice (1968) as in Eq. (1) by applying Green Theorem for any closed curve, Γ* as follows:

$$\int_{\Gamma^*} \left(W dy - \vec{T} . \frac{\partial u}{\partial z} ds \right) = 0 \quad (3)$$

The use of SIF concept is limited for elastic analysis only and it is successfully used to characterize high strength and low toughness materials. For ductile materials, SIF approaches cannot be used since the effect of plasticity is not included. SIF can be converted into J-integral if the material used is elastic as follows (Kim *et al.*, 2002):

$$J_e = \frac{K_x^2}{E}(1-\nu^2) \quad (4)$$

where, J_e is a elastic J-integral and K is a SIF and x represent the mode of loading. For Stress Intensity Factor (SIF), K, it can be defined as follows:

$$K_{I,a} = F_{I,b}\sigma_a\sqrt{\pi a} \quad (5)$$

$$K_{I,b} = F_{I,b}\sigma_a\sqrt{\pi a} \quad (6)$$

$$K_{II} = F_{II}\tau\sqrt{\pi a} \quad (7)$$

$$K_{III} = F_{III}\tau\sqrt{\pi a} \quad (8)$$

where, $K_{I,a}$, $K_{I,b}$ and K_{II}/K_{III} are the SIFs subjected to axial, bending and torsion loadings, respectively. $F_{I,a}$, $F_{I,b}$ and F_{II}/F_{III} are the respective correction factors for each loadings. The J-integral estimation for elastic-plastic analysis is the summation of elastic J-integral, J_e and elastic-plastic J-integral, J_p as follows:

$$J = J_e + J_p \quad (9)$$

J_e is defined as in Eq. (4). While, J_p is expressed as (Lei, 2004):

$$J_p = \alpha\varepsilon_o\sigma_o Dh\left(\frac{T}{T_L}\right)^{n+1} \quad (10)$$

where, α and n is a material constant and strain hardening exponent, respectively. T is an applied torsion and T_L is a normalizing torsion or limit load. ε_o is a yield strain and σ_o is yield stress. The symbol of h represents as fully plastic calibration and it is also called h-function. Moreover, Lei (2008) stated that the h-function solution for a surface crack in round bar is limited and lot of works need to be conducted.

In order to determine h-function, a relationship between J-integral obtained using finite element method, $J_{p\text{-}FE}$ and normalizing plastic J-integral, $J_{p\text{-}normal}$ is plotted. Then, the relations are represented by a linear function and the slope of each line is called h-function. It is dependent of crack aspect ratio, a/b, relative crack depth, a/D, normalized coordinate, x/h and strain hardening exponent, n. In order to minimize the numerical error, higher load level is only considered and low load level is omitted. This is due to the fact that, h-function is a fully plastic parameter. Therefore, Eq. (11) can be expressed as follows:

$$h_{III}\left(\frac{a}{b},\frac{a}{D},\frac{x}{h},n\right) = \frac{J_{P-FE}}{\alpha\varepsilon_o\sigma_o D\left(\frac{T}{T_L}\right)^{n+1}} = \frac{J_{p-FE}}{J_{p-normal}} \quad (11)$$

Crack modelling: The geometry of the crack shown in Figure 2 can be described by the dimensionless parameters a/D and a/b, the so-called relative crack depth and crack aspect ratio, respectively, where D, a and b are the diameter of the bar, the crack depth and the major diameter of the ellipse.

In this study, a/b is ranging between 0.0 to 1.2, while, a/D is in the range of 0.1 to 0.6 which are based on the experimental observations. Any arbitrary point, P on the crack front can also be normalised through the ratio of x/h, where h is the crack width and x is the arbitrary distance of P. The outer diameter of the cylinder is 50 mm and the total length is 200 mm. A finite element model is developed using ANSYS and a special attention is paid to the crack tip by employing 20-node iso-parametric quadratic brick elements. The

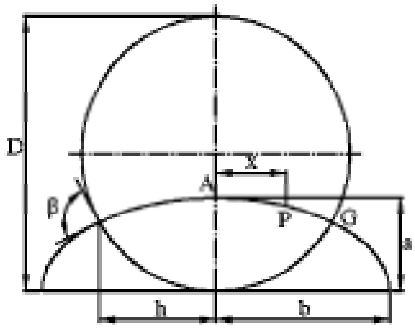

Fig. 2: Arbitrary crack shapes

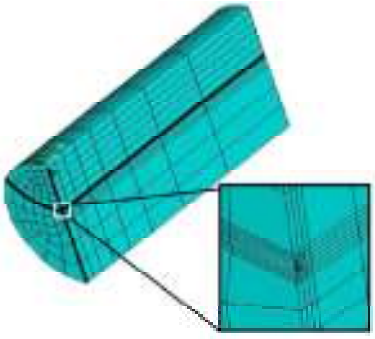

Fig. 3: A quarter finite element model for surface crack

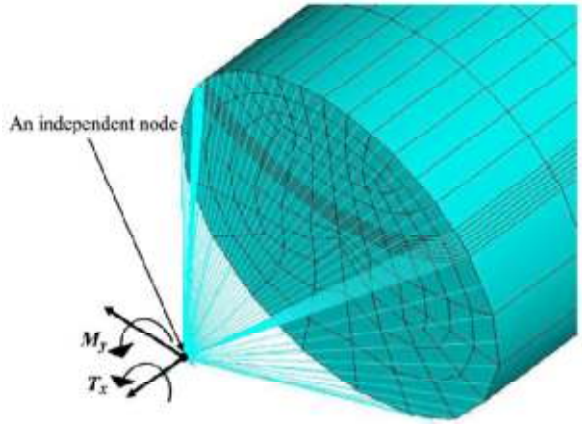

Fig. 4: A remotely applied moments to the bar

square-root singularity of stresses and strains is modelled by shifting the mid-point nodes to the quarter-point locations around the crack-tip region. A quarter finite element models is shown in Fig. 3.

In order to remotely apply loadings on the structural component, a rigid element or Multi-Point Constraint (MPC) is used to connect the nodes at a circumferential line at the end of the component to an independent node. Figure 4 shows a technique of constructing the independent node connected to the model using a rigid beam element. The bending moment, *My* and the torsion moment, *Tx*, are directly applied to this node, whereas the axial force, *F* is

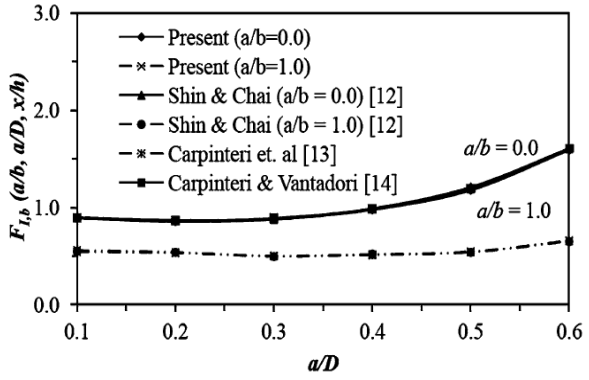

(a)

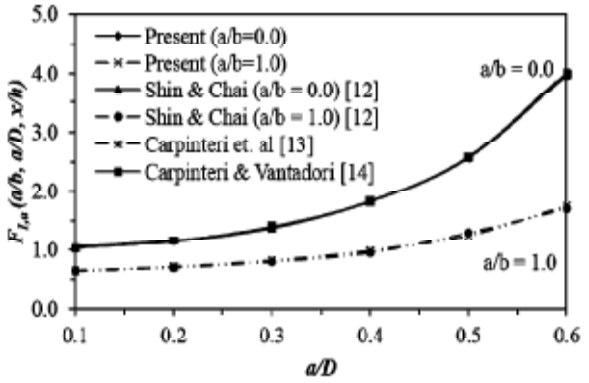

(b)

Fig. 5: Finite element model validation, (a) bending, (b) tension loadings

directly applied to the direction-*x* on the cross-sectional area of the round bar. At the other end, the component is constrained appropriately. In order to obtain a suitable finite element model, it is needed to compare the proposed model with others available in the literature (Shin and Chai, 2004; Carpinteri and Vantadori, 2009).

Figure 5 shows a comparison of the dimensionless SIFs under bending and tension loadings. Two crack aspect ratio, *a/b* used for the validation purposes, namely 0.0 and 1.0. It has been found that the findings of this study are in agreement with those determined by the previous models where the curves have coincident to each others. The solution of Mode III SIFs is difficult to obtain (Ismail *et al.*, 2011a) and consequently compare with the present results. Therefore, it can be assumed that the present model is also suitable to analyse Mode III condition in a satisfactory way. In order to model elastic-plastic for material, multi-linear isotropic hardening rule is used when it is combined with von Mises criterion associated with isotropic hardening and flow rule. Strain-stress relationship is characterized using Ramberg-Osgood equation. There are two type of strain hardening exponent are used

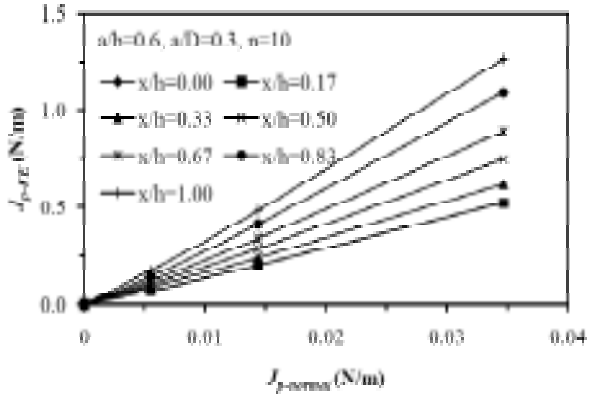

Fig. 6: Relations between $J_{p\text{-}FE}$ and $J_{p\text{-}normal}$ for a/b = 0.6, a/D = 0.3

n = 5 and 10. These values represent higher and lower strain hardening of such material.

RESULTS AND DISCUSSION

Mode III J-integral: Figure 6 shows the relation between plastic J-integral, $J_{p\text{-}FE}$ obtained using Finite Element Method (FEM) and normalizing plastic J-integral, $J_{p\text{-}normal}$ subjected to torsion moment for seven points along the crack front. Due to similar pattern of lines are observed, the results of a/b = 0.6, a/D = 0.3 and n = 10 are considered. The slopes of these lines are then calculated and it is represented as h-function. In this study, higher J-integral values are taken into account while lower J-integral or elastic J-integral is omitted. This is due to the fact that h-function is a fully plastic parameter.

Characteristics of these linear relations of h-function under mode III loading are different when compared with the results obtained using mode I loading (Ismail *et al.*, 2013). It is shown that the slopes increased with increasing x/h. This is due to the different in stress distribution subjected to mode III loading where the maximum stress occurred at the outer surface and the minimum stress at a middle point. Stress gradient around the cylindrical solid bars have affected the determination of h-function when compared with mode I loading. For further discussion, a crack geometry with a/b = 0.6 is considered due to typical pattern of linear relations for other crack. Figure 7 shows the mode III h-function plotted against x/h for cracks with a/b = 0.6, 0.8 and 1.0. Other types

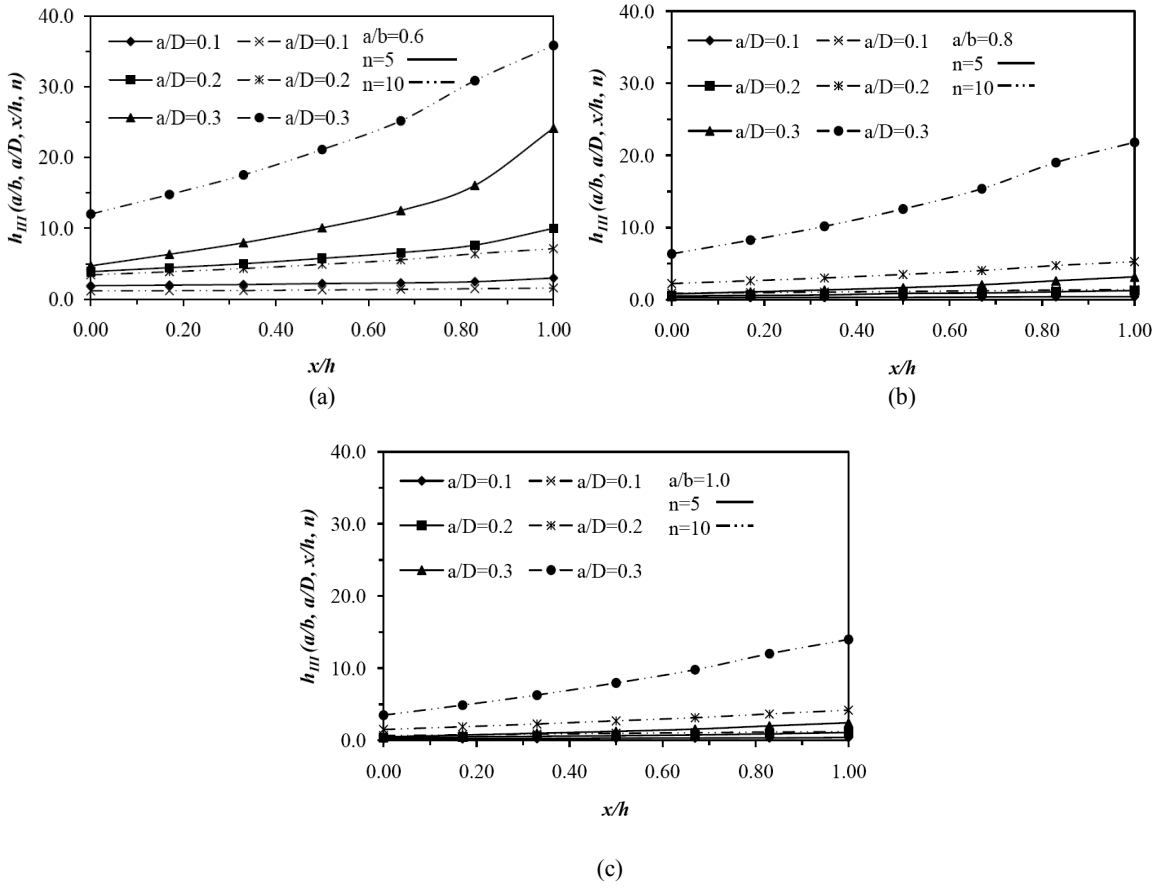

Fig. 7: Effect of h-function against x/h for (a) a/b = 0.6, (b) a/b = 0.8 and (c) a/b = 1.0

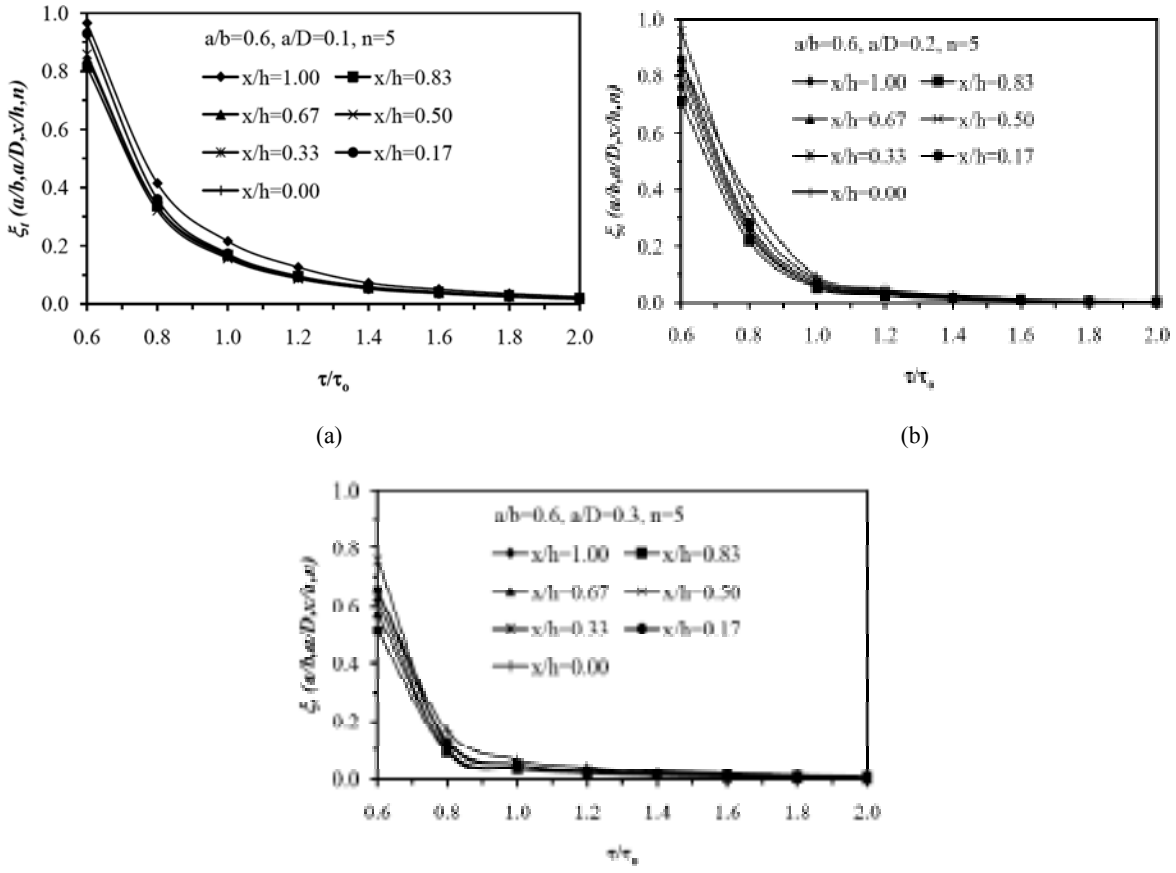

Fig. 8: The behavior of ξ_t against τ/τ_o of a/b = 0.6 and n = 5 for different a/D (a) 0.1, (b) 0.2 and (c) 0.3

of crack are not considered due to typical curves of *h*-function and the only difference is the values where it is increased when *a/D* is increased. Figure 7 (a) depicts the behavior of *h*-function for *a/b* = 0.6. For crack depth *a/D*≤0.2, it is found that the results are almost identical even different values of *n* are used indicating that *n* is not affected the *h*-function significantly.

However, when *a/D*≥0.3 is used, the different among the results are obviously significant. It is indicated that the shallow cracks (*a/D*≤0.2) capable to constraint any distortion due to the bar deformation even different *n* is used. When *a/D* reached certain depth (*a/D*≥0.3), *n* played an important role in determining crack deformation and consequently affected the *J*-integral calculations. It is shown that with increasing *a/D*>0.3, the use of *n* = 10 sustained to deform material easily and then producing higher *J*-integral along the crack front.

Similar curves can also be observed for others *a/b* as shown in Fig. 7b and c. However, increasing *a/b* caused *h*-function to decrease. This is due to the crack geometries used. If *a/b*>1.0 is considered, crack width is relatively shorter than the crack depth. This condition increased the cross-sectional area of the bar compared with *a/b*<1.0. Increasing such area produced higher bar resistance to the loading applied and then reducing *J*-integral along the crack front. According to literature survey (Lei, 2008), there are no solution for *h*-function subjected to mode III loading currently. Therefore, no validation of the present results can be conducted and it is solely dependent on the validation using elastic results such as stress intensity factors as in Fig. 5.

Limit load for torsion moment: Figure 8 and 9 show the normalized limit load under torsion moment, ξ_t for strain hardening exponent, *n* = 5 and 10, respectively which are plotted against normalized stress, τ/τ_o. It is found that when different *a/b* is considered, the pattern of limit load are almost identical where it is decreased asymptotically as τ/τ_o increased. Therefore, the crack with *a/b* = 0.6 is emphasized. Figure 8 reveals that it can be divided into two main regions which is lower load region (τ/τ_o<1.0) and higher load region (τ/τ_o>1.0). In the area of τ/τ_o<1.0, it is found that the higher distribution of limit load can be observed when compared with the area of τ/τ_o>1.0 indicated that elastic *J*-integral influenced the determination of limit

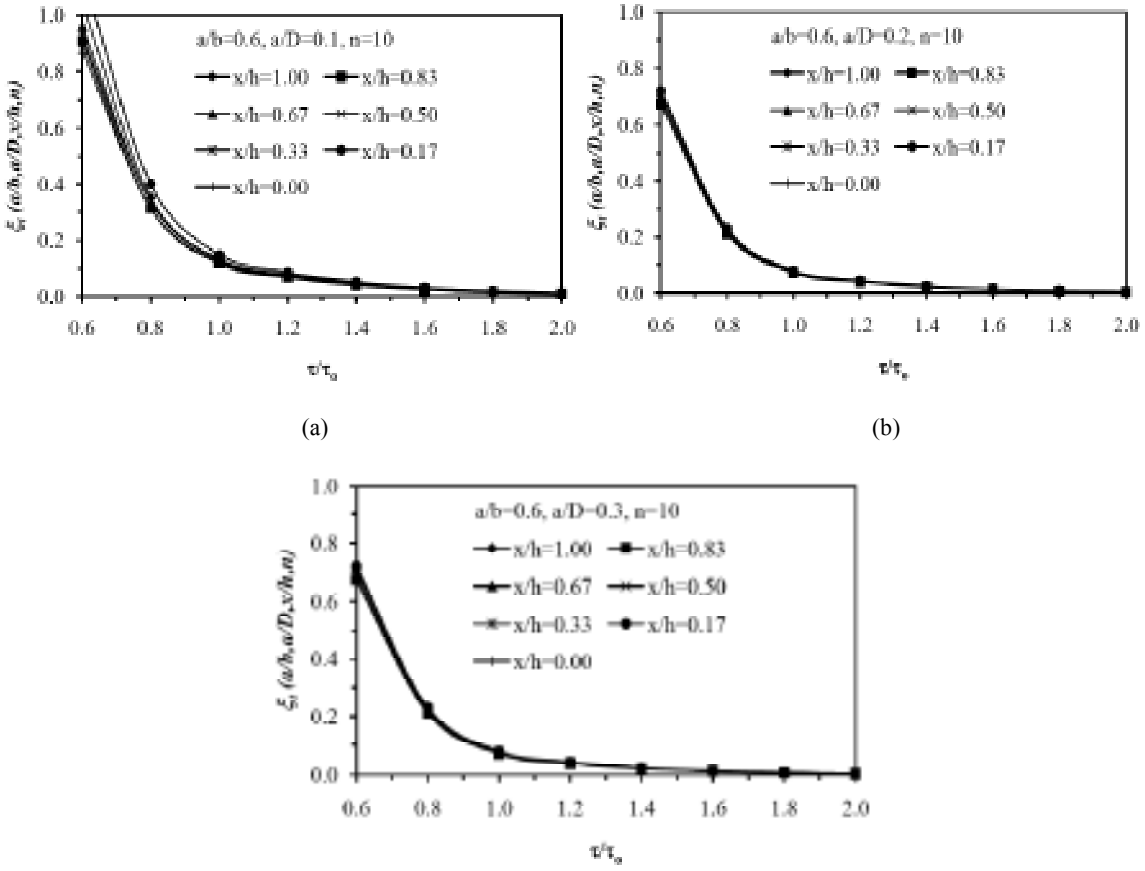

(a) (b)

(c)

Fig. 9: The behavior of ξ_t against τ/τ_o of a/b = 0.6 and n = 10 for different a/D (a) 0.1, (b) 0.2 and (c) 0.3

load, ξ_t. These type of curves showed that the overall deformation of the entire bar subjected to torsion moment is dominated by the elastic *J*-integral, J_e. Additionally, J_e is not relevant in determining *h*-function which is a fully plastic parameter.

Increasing τ/τ_o indicated the large distribution of limit load gradually decreased where all curves have closed to each others. The plastic deformation increased and the present limit load is then affected significantly where the limit load of each specified crack condition become a merged lines. For cracks with n = 10 as in Fig. 9 found that there is no significant different between two distinct regions. This is indicated that those materials are easily deformed and consequently plastic *J*-integral dominated along the crack front. Therefore, *h*-function curves are overlapped indicating that only a single limit can be used to represent various types of cracks.

J-integral estimation formulation: Limit load behavior under mode III in Fig. 8 and 9 can be described by observing the curve characteristics of *J*-integral ratio, J/J_e along the crack front. Mathematically, the prediction of J-integral can be conducted by substituting Eq. (4) and (7) into (6) as follows:

$$\frac{J\left(\frac{x}{h}\right)}{J_e\left(\frac{x}{h}\right)} = 1 + \frac{9\alpha\left(\frac{3}{4}\frac{\tau}{\tau_o}\right)^{n-1}}{8\pi\left(\frac{a}{R}\right)\left(1-\nu^2\right)}\left(\frac{h_{III}\left(\frac{x}{h}\right)}{F^2_{II-III}\left(\frac{x}{h}\right)}\right) \quad (12)$$

where, $J = J_e + J_p$. It is found the parameter *x/h* can be varied and other parameters are assumed constant. Therefore, J/J_e is determined using parameter $h_{III}/F^2_{II\text{-}III}$ for various types of cracks. The behavior of $h_{III}/F^2_{II\text{-}III}$ which are plotted against *x/h* for n = 5 and 10 as in Fig. 10 and 11, respectively. The curves of $h_{III}/F^2_{II\text{-}III}$ obtained using mode III are obviously different compared with the results of $h_{III}/F^2_{I,b}$ under bending moment and $h_{III}/F^2_{I,a}$ under tension force (Ismail *et al.*, 2011b, 2012b). Figure 10 shows the overall effect of $h_{III}/F^2_{II\text{-}III}$ against *x/h* when *a/D* is increased. For certain case, Fig. 10a reveals the curve behavior of *a/D* = 0.1. There is no flattened curve occurred along the crack front. It is indicated that $h_{III}/F^2_{II\text{-}III}$ increased with

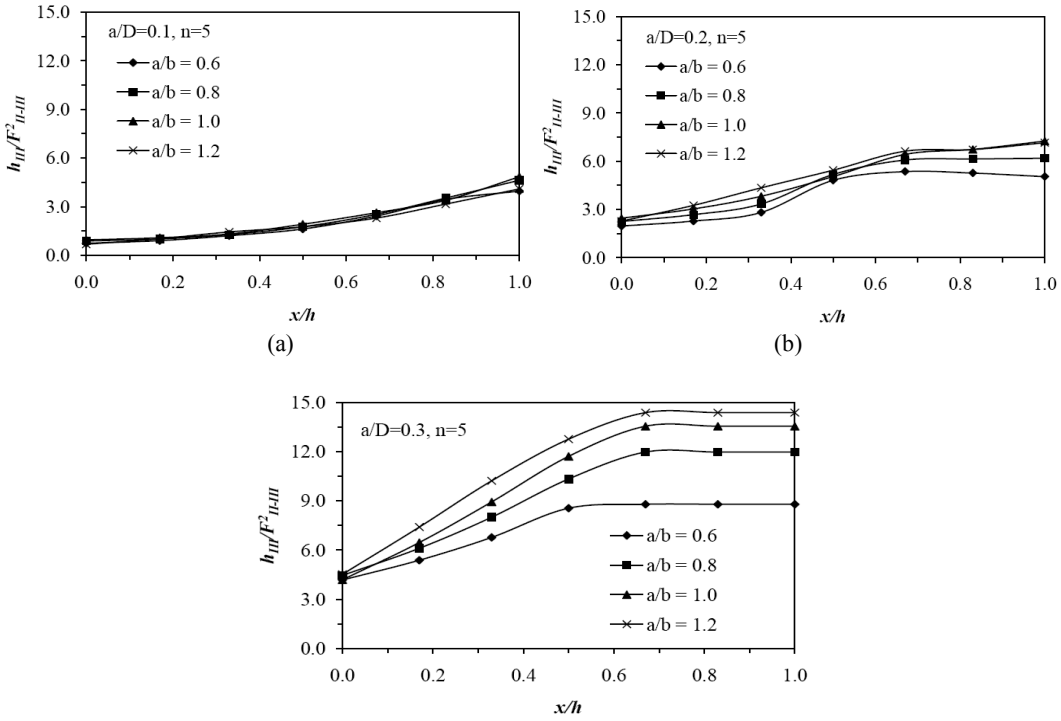

Fig. 10: The behavior of h_{III}/F^2_{II-III} against x/h of n = 5 and different a/b for a/D, (a) 0.1, (b) 0.2 and (c) 0.3

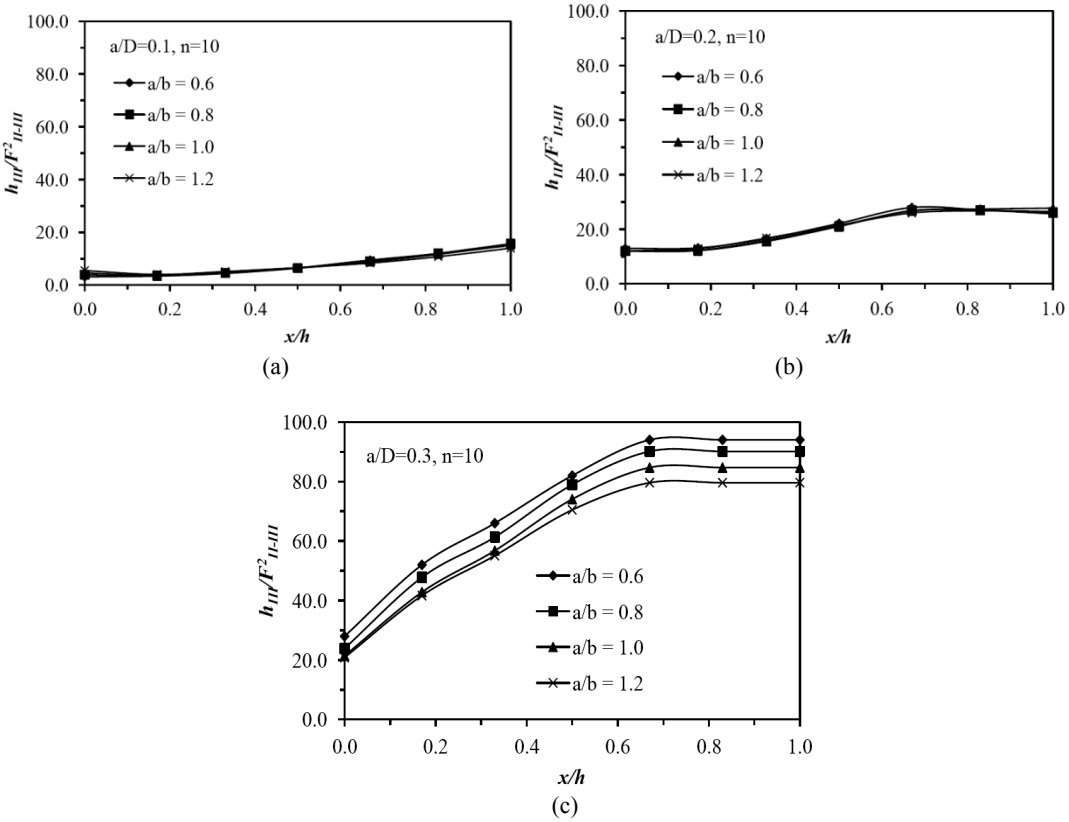

Fig. 11: The behavior of h_{III}/F^2_{II-III} against x/h of n = 10 and different a/b for a/D, (a) 0.1, (b) 0.2 and (c) 0.3

increasing x/h. Therefore, it is difficult to estimate the J-integral along the crack front using a single limit load.

It is also shown that different limit load must be used to predict the J-integral for different position along the crack front. This is due to the fact that when a/D = 0.1, it can be categorized as a shallow crack and it has higher bar resistance. This condition successfully prevented the plastic deformation around the crack tip and consequently reduced the formation of plastic J-integral. On the other hand, it is increased the elastic J-integral which is less relevant in determining the limit load which is a fully plastic parameter. However, when a/D is increased to 0.2, the curves of h_{III}/F^2_{II-III} are obviously changed as x/h increased. When it is reached at a certain position along the crack front (x/h>0.6), the curves flattened can be observed. This condition described where J-integral can be estimated using a single limit load. At the same time, in the region of x/h<0.6 where the curve is not well flattened, different limit load is used to determine the J-integral at different position along the crack front as in Fig. 10b and c.

The existent of two distinct regions are affected significantly whether it is an elastic or plastic dominated J-integral. For the region of x/h<0.6, it is found that the parameter h_{III}/F^2_{II-III} increased when x/h is increased. It is showed that the region is significantly affected by the elastic J-integral. On the other hand, the region of x/h>0.6, plastic J-integral is more dominant. Therefore, the curves for this region is flattened compared with the region of x/h<0.6. Similar behavior of h_{III}/F^2_{II-III} can be observed for the curves using n = 10 as shown in Fig. 11. Similar type of loading as used in obtaining the results as in Fig. 10. However, the crack induced significant amount of plastic J-integral along the crack front. Such plastic deformation along the crack front is due to the fact that the material with n = 10 has low resistant to mechanical deformation and consequently produced higher J-integral. Therefore, the curves obtained using n = 10 is higher than the curves of n = 5.

CONCLUSION

This study presents two approached which are finite element and analytical methods. Due to lack of J-integral solution available especially in obtaining h-function for surface crack in round bars. Therefore, ANSYS finite element method is utilized. On the other hand, a mathematical model to predict J-integral for surface crack is developed which is based on the reference stress approach. According to the present results, it is found that J-integral along the crack front can be estimated for various types of cracks. However, the J-integral prediction is successfully conducted except for the elastic-dominated region.

ACKNOWLEDGMENT

Author acknowledged University Tun Hussein onn Malaysia (UTHM) and Office for Research, Innovation, Commercialization and Consultancy management (ORICC) for sponsoring (Vot. 1001) this research and manuscript.

REFERENCES

Anderson, T.L., 2005. Fracture Mechanics: Fundamentals and Applications. 3rd Edn., Taylor and Francis, Boca Raton, FL.

Carpinteri, A. and S. Vantadori, 2009. Sickle-shaped cracks in metallic round bars under cyclic eccentric axial loading. Int. J. Fatigue, 31(4): 759-765.

Fonte, M.A. and M.M. Freitas, 1997. Semi-elliptical crack growth under rotating or reversed bending combined with steady torsion. Fatigue Fracture Eng. Mater. Structur., 20(6): 895-906.

Ismail, A.E., A.K. Ariffin, S. Abdullah, M.J. Ghazali and R. Daud, 2011a. Elastic-plastic analysis ofsurface crack in round bars under torsion. Key Eng. Mater., 462-463: 651-656.

Ismail, A.E., A.K. Ariffin, S. Abdullah, M.J. Ghazali and R. Daud, 2011b. Modes III stress intensity factors of surface crack in round bars. Adv. Mater. Res., 214:192-196.

Ismail, A.E., A.K. Ariffin, S. Abdullah and M.J. Ghazali, 2012a. Stress intensity factors for surface cracks in round bar under single and combined loadings. Meccanica, 47: 1141-1156.

Ismail, A.E., A.K. Ariffin, S. Abdullah, M.J. Ghazali, R. Daud and M. AbdulRazzaq, 2012b. Stress intensity factors under combined bending and torsion moments. J. Zhejiang Uni., Sci., A 13: 1-8.

Ismail, M.M., M.H. Gamaleldein and K.A. Hassa, 2013. Closed Kinetic Chain exercises with or without additional hip strengthening exercises in management of Patellofemoral pain syndrome: A randomized controlled trial. Eur. J. Phys. Rehabil. Med., (Epub Ahead of Print).

Kim, Y.J., N.S. Huh, Y.J. Park and Y.J. Kim, 2002. Elastic-plastic J and COD estimates for axial through-wall cracked pipes. Int. J. Pressure Vessels Piping, 79(6): 451-464.

Lei, Y., 2004. J-integral and limit load analysis of semi-elliptical surface cracks in plates under combined tension and bending. Int. J. Pressure Vessels Piping, 81(1): 31-41.

Lei, Y., 2008. A review of limit load solutions for cylinders with axial cracks and development of new solutions. Int. J. Pressure Vessel Piping, 85: 825-850.

Murakami, Y. and H. Tsuru, 1987. Stress Intensity Factor Handbook. Pergamon, New York.

Raju, I.S. and J.C. Newman, 1982. Stress-intensity factor for internal and external surface cracks in cylindrical vessels. Int. J. Pressure Vessels Technol., 104: 293-301.

Rice, J.R., 1968. A path independent integral and the approximate analysis of strain concentration by notches and cracks. J. Appl. Mech., 35: 379-386.

Shin, C.S. and C.Q. Cai, 2004. Experimental and finite element analyses on stress intensity factors of an elliptical surface crack in a circular shaft under tension and bending. Int. J. Fracture, 129(3): 239-264.

Shahani, A.R. and S.E. Habibi, 2007. Stress intensity factors in a hollow cylinder containing a circumferential semi-elliptical crack subjected to combined loading. Int. J. Fatigue, 29(1): 128-140.

Toribio, J., J.C. Matos, B. Gonzalez and J. Escuadra, 2009. Numerical modeling of crack shape evolution for surface flaws in round bars under tensile loading. Eng. Failure Anal., 16(2): 618-630.